PCCP

PAPER

Shock wave and modeling study of the thermal decomposition reactions of pentafluoroethane and 2-*H*-heptafluoropropane

Cite this: *Phys. Chem. Chem. Phys.*, 2014, **16**, 9797

C. J. Cobos,[a] L. Sölter,[b] E. Tellbach[b] and J. Troe*[bc]

Received 10th October 2013,
Accepted 15th November 2013

DOI: 10.1039/c3cp54274b

www.rsc.org/pccp

The thermal decomposition reactions of CF_3CF_2H and CF_3CFHCF_3 have been studied in shock waves by monitoring the appearance of CF_2 radicals. Temperatures in the range 1400–2000 K and Ar bath gas concentrations in the range (2–10) $\times 10^{-5}$ mol cm^{-3} were employed. It is shown that the reactions are initiated by C–C bond fission and not by HF elimination. Differing conclusions in the literature about the primary decomposition products, such as deduced from experiments at very low pressures, are attributed to unimolecular falloff effects. By increasing the initial reactant concentrations in Ar from 60 to 1000 ppm, a retardation of CF_2 formation was observed while the final CF_2 yields remained close to two CF_2 per C_2F_5H or three CF_2 per C_3F_7H decomposed. This is explained by secondary bimolecular reactions which lead to comparably stable transient species like CF_3H, releasing CF_2 at a slower rate. Quantum-chemical calculations and kinetic modeling help to identify the reaction pathways and provide estimates of rate constants for a series of primary and secondary reactions in the decomposition mechanism.

1. Introduction

CF_3H, C_2F_5H, and C_3F_7H have been proposed as fire suppressants, replacing the environmentally harmful halons (see, *e.g.*, ref. 1–5 and work cited therein). The use of these substances is not unproblematic as they have long atmospheric lifetimes and even may enhance combustion (see ref. 6 and work cited therein). For this reason, it appears to be obligatory to understand the mechanism and rates of the thermal decomposition of these substances. The proposed modeling schemes (see, *e.g.*, ref. 3, 6 and 7) contain a large number of estimated and uncertain rate constants, such that more detailed work appears to be desirable.

The present work focusses on the primary dissociation of C_2F_5H and C_3F_7H while in a previous publication[8] we reported studies of the primary dissociation of CF_3H. Besides the experiments, a modeling of the results in terms of unimolecular rate theory is required such that temperature and pressure dependencies of the rates can be characterized. In addition, quantum-chemical calculations about the different possible pathways of the primary dissociations and their transition state properties as well as of possible secondary reactions are necessary. Some quantum-chemical studies have been reported before, *e.g.* for C_2F_5H in ref. 9–11, and for C_3F_7H in ref. 5 and 12. The present work extends such calculations.

Previous experimental work on the pyrolysis of C_2F_5H is scarce. There has been the single-pulse shock tube study of ref. 13 and 14 over the range 1180–1470 K and pressures of 2980–4000 Torr and the turbulent flow study of ref. 10 over the range 1273–1373 K at atmospheric pressure. Much lower pressures (of the order of 10^{-4} to 10^{-3} Torr) were applied in a heated flow inside a UV photoelectron spectrometer,[5,11] allowing for an *in situ* analysis of primary reaction products. However, no attention was paid to possible pressure dependencies of the unimolecular dissociation steps. This will be done in the present work leading to different conclusions about primary products under practical conditions. Multiphoton dissociation studies of ref. 15 and 16 gave additional information on competing primary dissociation channels (see analogous experiments for $CF_3CF_2CHF_2$ in ref. 17). The pyrolysis results of ref. 10 and 14 differed considerably, *e.g.* by a factor of 5 in the dissociation rate constant at 1300 K, such that more work appears to be necessary. While the primary process in ref. 14 was believed to be HF elimination,

$$C_2F_5H\ (+\ M) \rightarrow C_2F_4 + HF\ (+\ M) \qquad (1)$$

some contribution of the bond breaking

$$C_2F_5H\ (+\ M) \rightarrow CF_2H + CF_3\ (+\ M) \qquad (2)$$

[a] *INIFTA, Facultad de Ciencias Exactas, Universidad Nacional de La Plata, Argentina*
[b] *Institut für Physikalische Chemie, Universität Göttingen, Tammannstrasse 6, D-37077 Göttingen, Germany. E-mail: shoff@gwdg.de*
[c] *Max-Planck-Institut für Biophysikalische Chemie, Am Fassberg 11, D-37077 Göttingen, Germany*

was also postulated for the highest temperatures (above about 1350 K). In contrast to the single-pulse analysis technique used in ref. 13 and 14, the present shock wave study used UV absorption spectroscopy of CF_2 radicals to follow the reaction. CF_2 is either formed by the decomposition of C_2F_4 through

$$C_2F_4\ (+\ M) \rightarrow 2\,CF_2\ (+\ M) \qquad (3)$$

i.e. from the product of reaction (1), or by the decomposition of CF_2H through

$$CF_2H\ (+\ M) \rightarrow CF_2 + H\ (+\ M) \qquad (4)$$

Reactions of CF_3 formed by reaction (2) will also take place. While we studied the decomposition of C_2F_4 in recent work,[18] we are not aware of similar work for the decomposition of CF_2H. Monitoring CF_2 has the advantage that a much closer and more sensitive look at the primary reaction steps becomes possible than with the techniques used before. Quantum-chemical calculations in the present work could also be made with more advanced techniques than applied in some of the earlier work.

Previous experimental work on the pyrolysis of C_3F_7H again is scarce. As for C_2F_5H, there has been a single-pulse shock tube study[4] over the temperature range 1200–1500 K and at pressures between 16 and 18 atm. The flow system study of ref. 19 gave qualitative information on reaction products. Experiments at very low gas pressures (10^{-4} to 10^{-3} Torr) in a flow inside a UV photoelectron spectrometer[5] as for C_2F_5H allowed for *in situ* identification of products, however, only under very low pressure conditions, see above. The shock tube study of ref. 3 considered a 68-step mechanism to describe the pyrolysis. It assumed an initiation by the two steps

$$CF_3CHFCF_3\ (+\ M) \rightarrow C_3F_6 + HF\ (+\ M) \qquad (5)$$

and

$$CF_3CHFCF_3\ (+\ M) \rightarrow CF_3CHF + CF_3\ (+\ M) \qquad (6)$$

while

$$CF_3CHFCF_3\ (+\ M) \rightarrow CF_3CFCF_3 + H\ (+\ M) \qquad (7)$$

was also assumed to be possible. In the present work, again UV absorption spectroscopy of CF_2 was employed to monitor a reaction product which is close to the primary reaction and can, *e.g.*, directly be formed by dissociation of C_3F_6 or CF_3CHF such as discussed below. While detailed quantum-chemical calculations of the primary decomposition steps of C_3F_7H are already available from ref. 12, we extended such calculations to a number of primary as well as secondary reaction steps.

2. Experimental techniques and results

We studied the thermal dissociation of C_2F_5H and C_3F_7H in reflected shock waves in a shock tube which has been described before.[8,18,20,21] We followed the progress of the reaction by monitoring the UV absorption of CF_2 at 248 nm. Due to the strong absorption of this species, we were able to work with highly diluted reaction mixtures, down to 60 ppm of reactant concentrations in the bath gas Ar. The study of the concentration dependence of CF_2 formation turned out to be of crucial importance for an understanding of the overall mechanism. Argon of high purity (>99.999% from Air Liquide) was used while less high purity (>99.7% from abcr) appeared to be sufficient for C_2F_5H and C_3F_7H. Experiments were done over the range 1400–2000 K while Ar concentrations in the present experiments were in the range (2–10) $\times$ 10^{-5} mol cm^{-3}, corresponding to pressures in the range 3–12 bar. For more details of our technique, see ref. 8, 18, 20 and 21.

An essential condition for our studies was the precise knowledge of the absorption coefficient ε of CF_2 (base e) at the observation wavelength 248 nm. We have redetermined ε in ref. 18 in our studies of the dissociations of C_2F_4 and CF_3H, both of which are particularly direct precursor molecules of CF_2. Within an estimated precision of about $\pm$10 percent, we obtained the temperature dependence of ε as

$$\varepsilon(\lambda = 248\ \text{nm}, T)/\text{cm}^2\ \text{mol}^{-1} = 3.35 \times 10^6 + 4.6 \times 10^7 \times \exp\{-[(T + 1457\ \text{K})/1272\ \text{K}]^2\} - 245 \times (T/\text{K}) \qquad (8)$$

With this calibration of ε we could show that (within 10% uncertainty) C_2F_5H decomposition under our conditions finally leads to 2 CF_2 radicals while C_3F_7H decomposition leads to 3 CF_2 radicals. One would be tempted to conclude from these results that reaction (1) followed by the faster reaction (3) dominates C_2F_5H decomposition. Likewise, one might conclude that C_3F_7H decomposition is dominated by reaction (5) followed by the faster dissociation of C_3F_6 to 3 CF_2. However, our detailed studies of the concentration dependence of the kinetics of CF_2 formation showed that this conclusion is premature and a more complicated mechanism of radical reactions has to be considered.

Fig. 1 shows the appearance of CF_2 radicals during the decomposition of C_2F_5H behind a reflected shock at 1655 K

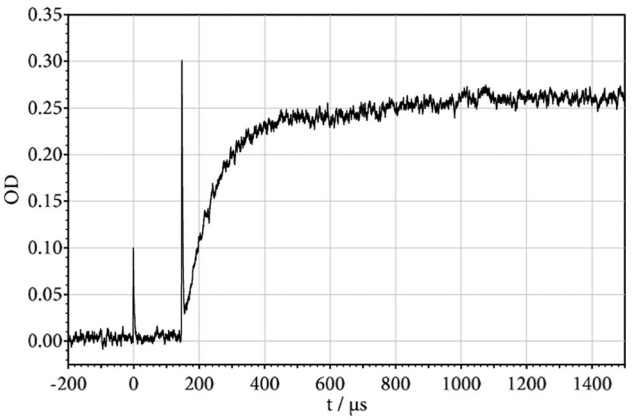

Fig. 1 CF_2 formation in the decomposition of C_2F_5H (OD = absorbance of CF_2 at 248 nm, spikes = Schlieren signals at the arrival of the incident and reflected shocks, reflected shock conditions: T = 1655 K, [Ar] = 8.2 $\times$ 10^{-5} mol cm^{-3}, initial reactant concentration = 72 ppm).

and [Ar] = 8.2 × 10^{-5} mol cm^{-3}. The formation of CF_2 here nearly follows a first order rate law

$$[CF_2] = [CF_2]_{t=\infty}[1 - \exp(-k_a t)] \quad (9)$$

with $[CF_2]_{t=\infty}$ being close to $2[C_2F_5H]_{t=0}$. An initial concentration $[C_2F_5H]_{t=0}$/[Ar] of only 7.2 × 10^{-5} = 72 ppm was employed here. Over the range [Ar] = (2–10) × 10^{-5} mol cm^{-3}, within our accuracy of ±10% in k_a we could not detect a major pressure dependence of k_a. However, there are indications that the derived value of k_a nevertheless is below the high pressure limiting value of the rate constant, see below.

Experiments like those of Fig. 1 were done also for C_3F_7H decomposition. Fig. 2 shows an absorption-time profile for this reaction at T = 1474 K, [Ar] = 9.5 × 10^{-5} mol cm^{-3}, and $[C_3F_7H]_{t=0}$/[Ar] = 67 ppm. In this case the final CF_2 yield is close to $3[C_3F_7H]_{t=0}$. The corresponding first order rate constant in eqn (9) is called k_b. Within our experimental uncertainty, we again could not detect a major pressure dependence of k_b. However, the same remark about the relation between k_b and its high pressure limiting value applies as for k_a, see above.

Fig. 1 and 2 were obtained with reactant concentrations of around 70 ppm in the carrier gas Ar. Extending such experiments to lower temperatures, some deviations from the simple time law of eqn (9) were observed. Fig. 3 shows an example. After a relative long induction time some acceleration of the formation of CF_2 just becomes noticeable. We come back to this observation later. Extending the experiments to higher temperatures, on the other hand, also some minor consumption of CF_2 was observed after the formation of CF_2 from the primary dissociation was complete, see an illustration given below. We also discuss this observation later.

Increasing the reactant concentration from values near 70 ppm to values in the range 500–1000 ppm, an interesting and unusual change of the rate law was observed both for C_2F_5H and C_3F_7H decompositions. The apparent rates of CF_2 formation decreased noticeably, while the final CF_2 yields remained unchanged near $2[C_2F_5H]_{t=0}$ and $3[C_3F_7H]_{t=0}$, respectively. In addition, some deviations from the simple first order rate law of eqn (9) became apparent. One can best illustrate these

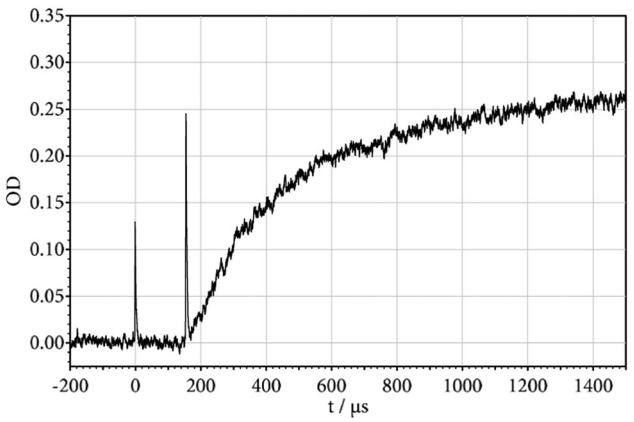

Fig. 2 CF_2 formation in the decomposition of C_3F_7H (as Fig. 1, but T = 1474 K, [Ar] = 9.5 × 10^{-5} mol cm^{-3}, initial reactant concentration 67 ppm).

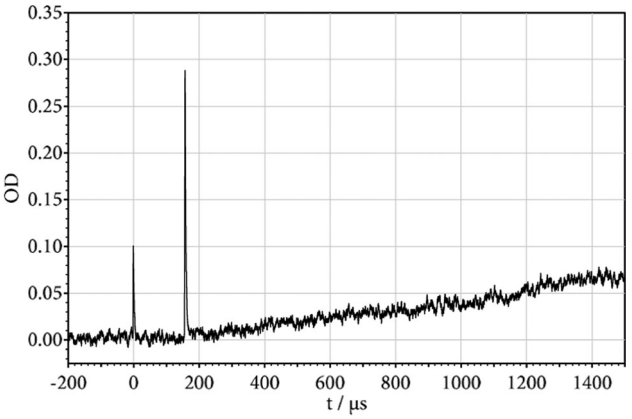

Fig. 3 As Fig. 1, with T = 1432 K, [Ar] = 9.5 × 10^{-5} mol cm^{-3}.

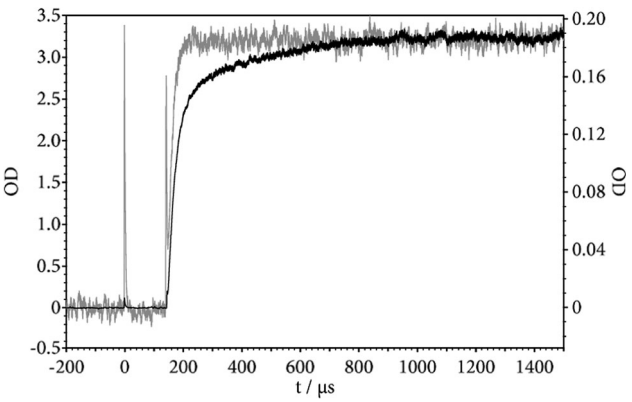

Fig. 4 Comparison of CF_2 formation in "low concentration-" (70 ppm, grey trace) and "high concentration-" (1000 ppm, black trace) experiments for C_2F_5H near T = 1800 K and [Ar] = 5 × 10^{-5} mol cm^{-3}.

observations by comparing in one picture the "low"- and "high-concentration" absorption-time profiles after scaling the CF_2 absorptions to the final CF_2-levels. Fig. 4 shows an example for C_2F_5H decomposition near 1800 K. In the same way, Fig. 5 in addition illustrates the observation of some short-time consumption of CF_2 in low-concentration experiments at higher temperatures (here near 2000 K), such as discussed later.

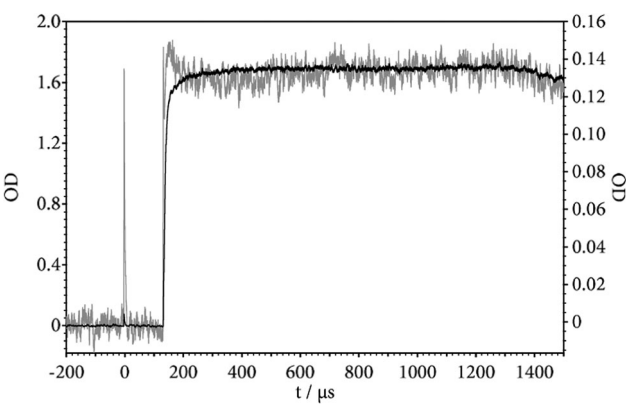

Fig. 5 As. Fig. 4, but near T = 2000 K.

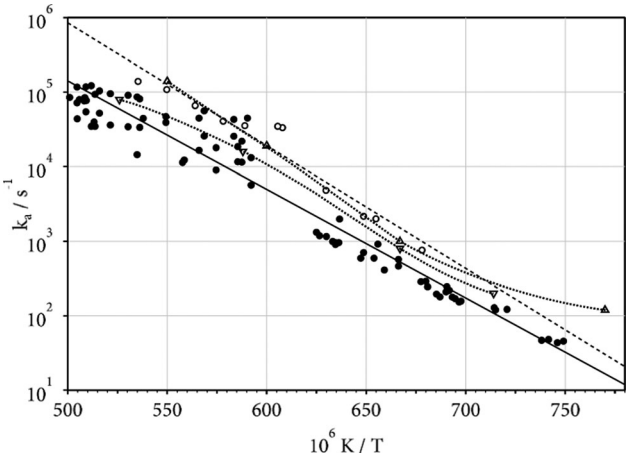

Fig. 6 Temperature dependence of "low-concentration" ($k_{a,l}$, 70 ppm) and "high-concentration" ($k_{a,h}$, 600 and 1000 ppm) rate constants k_a for CF_2-formation in C_2F_5H decomposition (at [Ar] = 5×10^{-5} mol cm^{-3}). (Open circles: 70 ppm, filled circles: 600–1000 ppm of C_2F_5H in Ar; dashed line: $k_{a,l}$ from eqn (11); full line: $k_{a,h}$ from eqn (13); dotted line with △: $k(C_2F_6 \rightarrow 2\ CF_2)$ at the same [Ar] from ref. 21, dotted line with ▽: $k(CF_3H \rightarrow CF_2 + HF)$ at the same [Ar] from ref. 8, see the text).

A comparison of "low"- and "high"-concentration rate constants $k_{a,l}$ and $k_{a,h}$, respectively, is given in the Arrhenius plot of Fig. 6. The lowering of the apparent first-order rate constants from $k_{a,l}$ (at 70 ppm) to $k_{a,h}$ (at 600 and 1000 ppm) is significant. The figure also includes rate constants[21] for the C–C bond breaking in $C_2F_6 \rightarrow 2\,CF_3$ at the same Ar concentration of about 5×10^{-5} mol cm^{-3} such as used in most of the present experiments. At the same time, it includes rate constants[8] for CF_2 formation in $CF_3H \rightarrow CF_2 + HF$, again at [Ar] = 5×10^{-5} mol cm^{-3}. A relation of the rate constants for C_2F_6 and CF_3H decompositions to $k_{a,l}$ and $k_{a,h}$, respectively, will be discussed later. (One should note that a decrease of the rate constants for C_2F_6 and CF_3H decompositions by falloff effects in Fig. 6 has been accounted for.)

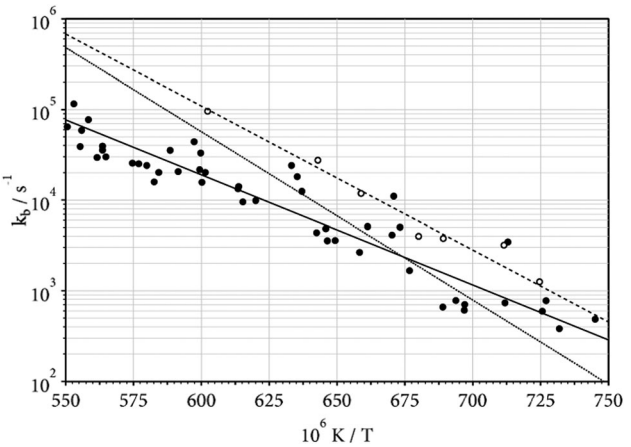

Fig. 7 Rate constants k_b (analogous to Fig. 6), for CF_2-formation in C_3F_7H decomposition (at [Ar] = 8.5×10^{-5} mol cm^{-3}). (Open circles: 60 ppm, filled circles: 260–500 ppm of C_3F_7H in Ar; dashed line: $k_{b,l}$ from eqn (12); full line: $k_{b,h}$ from eqn (14); dotted line: $k(C_3F_7H \rightarrow CF_3CHF + CF_3)$ as fitted in ref. 3).

Fig. 7 shows analogous results for C_3F_7H. All CF_2-profiles were fitted to eqn (9) such that the shown values of k_a and k_b are apparent values only, as there were the described deviations from eqn (9). We note that we observed the transition between $k_{a,l}$ and $k_{a,h}$ (or $k_{b,l}$ and $k_{b,h}$) over the concentration range of our experiments, while the limiting values of $k_{a,l}$ and $k_{a,h}$ (or $k_{b,l}$ and $k_{b,h}$) apparently did not further depend on the concentration. For experimental reasons, we did not further inspect more details of the transition between $k_{a,l}$ and $k_{a,h}$. However, as shown in Fig. 6 we note that $k_{a,l}$ is close to $k(C_2F_6 \rightarrow 2\,CF_3)$ while $k_{a,h}$ is close to the rate constant for the reaction

$$CF_3H\ (+\ M) \rightarrow CF_2 + HF\ (+\ M) \qquad (10)$$

The latter observation provides a key to the understanding of our results such as given below. Our rate constants $k_{a,l}$, $k_{b,l}$, $k_{a,h}$, and $k_{b,h}$ can be represented approximately by the Arrhenius expressions

$$k_{a,l} \approx 1.4 \times 10^{14} \exp(-37\,910\ \mathrm{K}/T)\ \mathrm{s}^{-1} \qquad (11)$$

$$k_{b,l} \approx 3.5 \times 10^{11} \exp(-26\,270\ \mathrm{K}/T)\ \mathrm{s}^{-1} \qquad (12)$$

$$k_{a,h} \approx 2.8 \times 10^{12} \exp(-33\,580\ \mathrm{K}/T)\ \mathrm{s}^{-1} \qquad (13)$$

$$k_{b,h} \approx 1.6 \times 10^{9} \exp(-19\,930\ \mathrm{K}/T)\ \mathrm{s}^{-1} \qquad (14)$$

We note that, for [Ar] = 5×10^{-5} mol cm^{-3}, the rate constant for reaction (10) from ref. 8 is represented by nearly the same expression as given by eqn (13). We emphasize, however, that $k_{a,l}$, $k_{a,h}$, $k_{b,l}$ and $k_{b,h}$ are composite values including the effects of several secondary reactions as well as pressure effects. Before further analyzing our experimental results, quantum-chemical calculations for possible reaction pathways and modeling of primary dissociation rates by unimolecular rate theory are described. The results help unraveling the observations.

3. Modeling of primary decomposition pathways

As the monitored CF_2 radicals are not primary decomposition products of C_2F_5H and C_3F_7H, one has to analyze their formation first by inspecting the primary decomposition pathways using quantum-chemical modeling. In part this has already been done in ref. 9–11 for C_2F_5H and in ref. 5 and 12 for C_3F_7H. In addition, however, we also need to consider the secondary processes which finally lead to CF_2. Again quantum-chemical calculations here are helpful to identify the most relevant pathways.

3.1 Decomposition of C_2F_5H

Density functional theory (DFT) and composite high-level *ab initio* methods were employed to estimate thermochemical and transition state properties of a variety of decomposition channels of C_2F_5H. Two DFT methods (BMK[22] and M06-2X[23]) combined with 6-311++G(3df,3pd) basis sets were used first. Afterwards, *ab initio* calculations were performed using the CBS-QB3 method[24] as well as the G3MP2B3,[25] G3B3,[25] G4MP2[26] and G4[27]

Table 1 Calculated reaction enthalpies for C_2F_5H decomposition channels in comparison to thermochemical values (at 0 K, in kJ mol^{-1}, see the text)

Reaction product	BMK[22]	M06-2X[23]	CBS-QB3[24]	G3B3[25]	G4[27]	Thermochem.[29]
$CF_3CF + HF$ (15)	333	337	326	324	318	—
$CF_2CF_2 + HF$ (16)	170	172	164	164	162	166
$CF_4 + CFH$ (17)	331	332	330	329	323	332
$CF_3H + CF_2$ (18)	220	230	226	226	220	232
$CF_3 + CF_2H$ (19)	389	397	406	405	392	410

Table 2 Calculated barrier heights for C_2F_5H decomposition channels (at 0 K, in kJ mol^{-1}, see the text)

Reaction product	BMK[22]	M06-2X[23]	CBS-QB3[24]	G3B3[25]	G4[27]
$CF_3CF + HF$ (15)	352	355	348	341	341
$CF_2CF_2 + HF$ (16)	364	369	373	367	368
$CF_4 + CFH$ (17)	544	536	538	532	534
$CF_3H + CF_2$ (18)	396	400	381	379	379
$CF_3 + CF_2H$ (19)	389	397	406	405	392

versions of Gaussian models. All calculations were carried out with the Gaussian 09 program.[28] We considered the primary decomposition channels

$$CF_3CF_2H \rightarrow CF_3CF + HF \quad (15)$$

$$CF_3CF_2H \rightarrow CF_2CF_2 + HF \quad (16)$$

$$CF_3CF_2H \rightarrow CF_4 + CFH \quad (17)$$

$$CF_3CF_2H \rightarrow CF_3H + CF_2 \quad (18)$$

$$CF_3CF_2H \rightarrow CF_3 + CF_2H \quad (19)$$

Table 1 compares computed reaction enthalpies with tabulated thermochemical data from ref. 29, while Table 2 presents computed transition state enthalpies for the corresponding reaction channels. We illustrate the corresponding energy profile in Fig. 8.

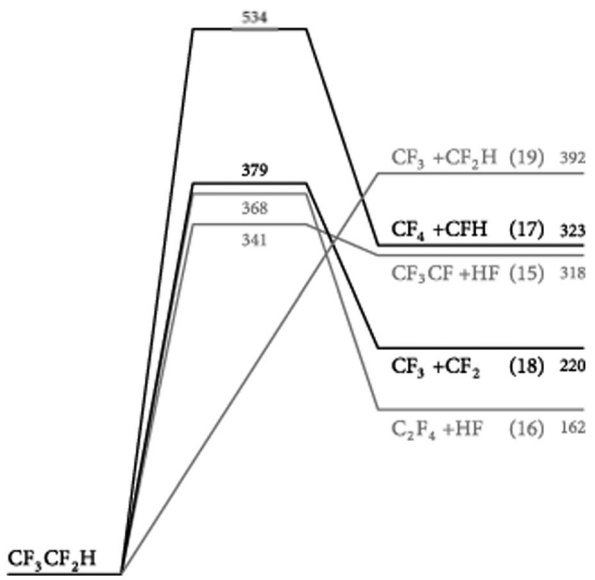

Fig. 8 Energy profile of the dissociation of C_2F_5H (quantum-chemical calculations with the G4 method, see Tables 1 and 2).

Inspecting Table 2 and Fig. 8 indicates that there are three elimination processes (reactions (15), (16) and (18)) which either directly or by fast secondary processes lead to CF_2. The electronic barrier for the isomerization

$$CF_3CF \rightarrow C_2F_4 \quad (20)$$

at the G3MP2B3 level was calculated to be 148 kJ mol^{-1}; therefore, this reaction is very fast. The secondary dissociation of C_2F_4 with its bond energy of ΔH_0° = 282 kJ mol^{-1}, on the other hand, is also fast enough[18] that the overall rate of CF_2 formation through reactions (15) and (16) would be governed by the rate of the latter processes. The three rigid-activated complex elimination processes (15), (16) and (18), however, compete with the loose-activated complex C–C bond breaking process (19). In the infrared multiphoton dissociation experiments of ref. 17, a dominance of reaction (19) over reaction (16) was found. Such a dominance in the thermal pyrolysis experiments of ref. 11 and 14 was suggested to be relevant only for temperatures above about 1350 K, while the opposite was postulated for lower temperatures.

In order to quantify the transition from a possible low-temperature rigid-activated complex elimination to a high-temperature loose-activated complex bond fission mechanism, we have further modeled the kinetics of reactions (15) and (19). Activated complex frequencies for reaction (15) were determined by DFT calculations such as given in the Appendix together with parent molecule frequencies. Rigid activated complex transition state theory then led to a high pressure rate constant

$$k_{15,\infty} \approx 5.5 \times 10^{14} \exp(-356 \text{ kJ mol}^{-1}/RT) \text{ s}^{-1}. \quad (21)$$

In view of the large pressure difference between the experiments of ref. 11 on one hand, and ref. 10 and 14, and the present work (10^{-4}–10^4 Torr), we also modeled[30–32] the low pressure rate constant $k_{15,0}$; in addition, broadening factors of the falloff curve as expressed by the center broadening factor $F_{\text{cent},15}$ were determined. Although the falloff curves turned out

to be very broad, with $F_{cent,15}$ being below 0.1 (at T > 1000 K), reaction (15) in contrast to reaction (10) under the conditions of the present work turned out to be close to its high pressure limit. We note that our modeled $k_{15,\infty}$ is closer to the results from ref. 10 ($k_{15,\infty}$(1300 K) = 2.7 s^{-1} from eqn (21), k_{15}(1300 K) = 7.6 s^{-1} from ref. 10) than to the results from ref. 14 (k_{15}(1300 K) = 37 s^{-1}). This discrepancy may have something to do with the different reactant concentrations employed. Similar to reaction (15) we modeled the high pressure rate constants for reactions (16) and (18) (reaction (17) being ruled out because of its high energy barrier, see Table 2). We obtained $k_{16,\infty} = 2.1 \times 10^{14} \exp(-389\ \text{kJ mol}^{-1}/\text{RT})\ \text{s}^{-1}$ and $k_{18,\infty} = 1.6 \times 10^{15} \exp(-399\ \text{kJ mol}^{-1}/\text{RT})\ \text{s}^{-1}$. This suggests that these two pathways would be considerably less important than reaction (15).

A comparison of the modeled $k_{15,\infty}$ with our measured $k_{a,l}$ from eqn (11), as well as the concentration dependence of the rate measurements described in Section 3.1, suggests that not the HF elimination process (15) but the C–C bond breaking process (19) dominates the decomposition under all of our conditions (perhaps except for temperatures below about 1400 K). The multiphoton dissociation experiments of ref. 15 and 16 support this conclusion. Energy-dependent specific rate constants $k(E)$ for this process in ref. 9 were compared with those for reaction (15). As these calculations were still tentative, and as we do not have sufficiently detailed knowledge about the potential energy surface for the bond-breaking in CF_3–CF_2H to repeat such calculations, here we rely on a comparison with the bond-breaking in CF_3–CF_3 analyzed in ref. 33. On the basis of pressure- and temperature-dependent experimental data for $CF_3 + CF_3$ (+ M) → C_2F_6 (+ M), in ref. 33 the high pressure rate constant for C_2F_6 decomposition was obtained. As the bond energy of CF_3–CF_3 of 410 kJ mol^{-1} (at 0 K) is practically identical with the value for CF_3–CF_2H (see ref. 29 and Table 1), we assume that the limiting high pressure dissociation rate constants are also nearly the same, *i.e.* we assume that $k_{19,\infty}$ is given by the value from ref. 33 for C_2F_6,

$$k_{19,\infty} \approx 2.2 \times 10^{18} (T/300\ \text{K})^{-0.52} \exp(-410\ \text{kJ mol}^{-1}/\text{RT})\ \text{s}^{-1} \quad (22)$$

Similar to C_2F_6, however, for reaction (19), under the present experimental conditions, we also expect reductions of k_{19} to values below $k_{19,\infty}$ due to falloff effects. Our modeling[29] of the limiting low pressure rate constants $k_{19,0}$ led to practically the same values as for $C_2F_6 \rightarrow 2\,CF_3$ from ref. 21. These can be represented by

$$k_{19,0} \approx [\text{Ar}]\ 4.3 \times 10^{34} (T/300\ \text{K})^{-13.8} \times \exp(-410\ \text{kJ mol}^{-1}/\text{RT})\ \text{cm}^3\ \text{mol}^{-1}\ \text{s}^{-1} \quad (23)$$

Furthermore, weak collision center broadening factors[30–32] of the falloff curves for 1300–2000 K were estimated with $F_{cent,19} \approx 0.04$. This indicates (see Fig. 3 of ref. 21) that k_{19} is about a factor of 3 below $k_{19,\infty}$ at [Ar] = 5 × 10^{-5} mol cm^{-3} and T = 1300 K while it is a factor of 5 below at T = 1500 K and a factor of 10 below at 1800 K. Fig. 6 includes the corresponding results for [Ar] = 5 × 10^{-5} mol cm^{-3} which well agree with our present ''low-concentration'' results $k_{a,l}$ (the line is nonlinear due to different falloff effects at different T, see ref. 21). Fig. 6 also includes k_{10} from ref. 8 (again its line is nonlinear due to different falloff effects at different T, see ref. 8).

The opposing conclusions about a dominance of the HF elimination reaction (15) from ref. 11 and about that of C–C bond breaking from the present work (and ref. 14) are easily explained by the described falloff effects. At 10^{-4} Torr and 1300 K, both reactions (15) and (19) are close to their low pressure limits where $k_{15,0}$, because of its smaller energy barrier and the reduction of the rate of energetically higher reaction channels in two-channel unimolecular reactions at low pressures,[34] becomes markedly larger than $k_{19,0}$. One could model this depletion effect by combining ref. 9 and 34 in order to estimate at which temperature, at the low pressure limit of the primary decomposition steps, the radical mechanism starts to dominate over the HF-elimination mechanism. This is not done here, because under practical conditions, *e.g.* of fire suppression, high pressure limiting rate constants are approached where $k_{15,\infty}$ is smaller than $k_{19,\infty}$, at least for T > 850 K, see eqn (21) and (22). As a consequence the product yields of C_2F_5H from the low pressure study of ref. 11 should not be considered for practical high pressure applications.

3.2 Decomposition of CF_3CFHCF_3

Quantum-chemical calculations of the thermochemistry and energy barriers have also been performed for various

Table 3 Calculated reaction enthalpies for C_3F_7H decomposition channels (at 0 K, * at 298 K, in kJ mol^{-1}, see the text)

Reaction product	BMK[22]	M06-2X[23]	CBS-QB3[24]	G3MP2B3[25]	G4MP2[26]	Ref. 12*
CF_3CFCF_2 + HF (24)	138	141	134	130	128	146
CF_3CCF_3 + HF (25)	409	410	407	393	387	401
CF_3H + CF_3CF (26)	341	355	353	348	339	343
CF_3CFH + CF_3 (27)	377	388	399	393	370	386

Table 4 Calculated barrier heights for C_3F_7H decomposition channels (at 0 K, *: at 298 K, in kJ mol^{-1}, see the text)

Reaction product	BMK[22]	M06-2X[23]	CBS-QB3[24]	G3MP2B3[25]	G4MP2[26]	Ref. 12*
CF_3CFCF_2 + HF (24)	322	325	329	326	326	333
CF_3CCF_3 + HF (25)	—	—	—	—	—	371
CF_3H + CF_3CF (26)	—	—	—	—	—	408
CF_3 CFH + CF_3 (27)	377	388	399	393	370	386

decomposition channels of C_3F_7H, employing the same methods as described in Section 3.1. Tables 3 and 4 summarize the results. The following pathways have been considered

$$CF_3CFHCF_3 \rightarrow CF_3CFCF_2 + HF \quad (24)$$

$$CF_3CFHCF_3 \rightarrow CF_3CCF_3 + HF \quad (25)$$

$$CF_3CFHCF_3 \rightarrow CF_3H + CF_3CF \quad (26)$$

$$CF_3CFHCF_3 \rightarrow CF_3CFH + CF_3 \quad (27)$$

(An energy profile analogous to Fig. 8, for this reaction, was already presented in ref. 12 and will not be repeated here). While reactions (24)–(26) are rigid-activated complex elimination reactions, the most favorable simple bond-breaking process is reaction (27). As for C_2F_5H, one has to discuss the temperature- and pressure-dependent competition between rigid- and loose-activated complex channels. The similarity of the concentration dependence of our apparent rate constants k_a and k_b again suggests the dominance of the radical-forming primary C–C bond-breaking process (27) for the employed pressures and over the complete temperature range 1300–1900 K of our study. One notices that the limiting low-concentration value of $k_{b,l}$ is roughly a factor of 10 larger than the corresponding value of $k_{a,l}$. This should be expected as the bond energy is about 18 kJ mol^{-1} (at 0 K) larger for reaction (19) than for reaction (27), and as reaction (27) should be closer to the high pressure limit of the unimolecular bond fission than reaction (19). The conclusion about a dominance of reaction (27) over the processes (24)–(26) is in accord with the results from the shock tube study of ref. 3 which were fitted by $k_{24} = 10^{12.9}\exp(-35\,000\ \mathrm{K}/T)\ \mathrm{s}^{-1}$ and $k_{27} = 10^{15.9}\exp(-42\,800\ \mathrm{K}/T)\ \mathrm{s}^{-1}$. With these data, reaction (27) would be slower than reaction (24) only at temperatures below 1120 K. On the other hand, ref. 5 found no evidence for reaction (27) between about 900 and 1500 K. Instead, reaction (24) was suggested to dominate up to about 1200 K, with reaction (25) becoming only important above about 1200 K. These opposing conclusions, however, again become reconcilable if one accounts for the large pressure differences of the two studies, ref. 3 applying 16–18 atm and ref. 5 working with 10^{-4} to 10^{-3} Torr. As discussed for C_2F_5H decomposition above, falloff effects in a two-channel unimolecular reaction with decreasing pressure here also reduce the rate constant of the energetically upper channel. The product yields measured in ref. 5, therefore, do not correspond to those relevant for high pressure practical applications.

We have also modeled the high pressure limiting rate constants of the rigid activated complex reactions (24)–(26) using the transition state properties of our own work and of ref. 12. With G4MP2 calculations we obtained $k_{24} \approx 3.6 \times 10^{15}\exp(-44\,300\ \mathrm{K}/T)\ \mathrm{s}^{-1}$, while with the *ab initio* results from ref. 12 we calculated $k_{25} \approx 5.8 \times 10^{14}\exp(-48\,600\ \mathrm{K}/T)\ \mathrm{s}^{-1}$ and $k_{26} \approx 3.5 \times 10^{14}\exp(-53\,000\ \mathrm{K}/T)\ \mathrm{s}^{-1}$ over the temperature range 1500–2500 K. All of these rate constants are markedly below our measured values for k_b, thus confirming the dominance of the bond-breaking reaction (27) over reactions (24)–(26) under the conditions of the present work.

4. Mechanism of primary and secondary reactions

4.1 Decomposition of C_2F_5H

In Section 3.1 it was shown that, at the lowest reactant concentrations (60 ppm) and for the present experimental temperatures and pressures, the dissociation of C_2F_5H is initiated by the C–C bond fission

$$C_2F_5H\ (+\ M) \rightarrow CF_2H + CF_3\ (+\ M) \quad (2)$$

The derived rate constants were found to agree with those of the reaction $C_2F_6\ (+\ M) \rightarrow 2\,CF_3\ (+\ M)$ which is energetically very close to reaction (19). We, therefore, recommend to identify k_{19} with the rate constant for C_2F_6 decomposition whose temperature- and pressure dependence was studied in more detail in ref. 33. Pressure-dependent Arrhenius expressions for k_{19} obtained in this way are given in ref. 33 such as also used in Fig. 6. Apparently, CF_2 formation at the lowest concentrations then occurs *via* the fast decomposition of CF_2H,

$$CF_2H\ (+\ M) \rightarrow CF_2 + H\ (+\ M) \quad (4)$$

and the slower decomposition of CF_3,

$$CF_3\ (+\ M) \rightarrow CF_2 + F\ (+\ M) \quad (28)$$

such that the overall reaction under low-concentration conditions is $C_2F_5H \rightarrow 2\,CF_2 + H + F$. Reaction (28) has, *e.g.*, been studied in ref. 21. It is not far from the low pressure limit of the unimolecular dissociation, having a rate constant $k_{28,0} \approx$ [Ar] $3.5 \times 10^{15}\exp(-249.6\ \mathrm{kJ\ mol^{-1}}/\mathrm{RT})\ \mathrm{cm^3\ mol^{-1}\ s^{-1}}$. For [Ar] $\approx 10^{-4}$ mol cm^{-3} and T = 1500 K, *e.g.*, $k_{28} \approx 7 \times 10^2\ \mathrm{s}^{-1}$, while $k_{19} \approx 3 \times 10^3\ \mathrm{s}^{-1}$. On the other hand, the F_2C–H bond energy at 0 K of 260 kJ mol^{-1} (from ref. 29, or 262.1 kJ mol^{-1} at the G4MP2 level) is considerably smaller than that of F_2C–F of 350 kJ mol^{-1} (from ref. 29, or 350.7 kJ mol^{-1} at the G4MP2 level) such that reaction (4) is much faster than reaction (19) and almost instantaneously leads to one CF_2 radical while the second CF_2 radical is produced on a somewhat slower time scale. Some indications for this delayed appearance of the second CF_2 possibly became apparent at the lower end of our temperature range, see Fig. 3.

Our experiments for the decomposition of C_2F_5H at higher reactant concentrations (1000 ppm) unexpectedly showed a slower rate of CF_2 appearance while the overall yield remained practically unchanged at two CF_2 formed per one C_2F_5H consumed. Quantum-chemical calculations help to identify the origin of this concentration effect. Endothermic secondary reactions like

$$CF_2 + CF_3CF_2H \rightarrow CF_2H + C_2F_5 \quad (29)$$

with ΔH_0° = 167.3 kJ mol^{-1} (at the G3MP2B3 level) and

$$CF_2 + CF_3CF_2H \rightarrow CF_3 + CF_3CFH \quad (30)$$

with $\Delta H_0^\circ \approx$ 109.7 kJ mol^{-1} (at the G4MP2 level) most probably can be ruled out under the present low concentration

conditions. On the other hand, one might consider a short chain starting with

$$H + CF_3CF_2H \rightarrow CF_3H + CF_2H \quad (31)$$

(with $\Delta H_0^o = -48.0$ kJ mol^{-1} at the G4MP2 level) and followed rapidly by reaction (4) which recycles H atoms, converts some C_2F_5H into CF_2 + CF_3H, and liberates the second CF_2 by the slower decomposition of CF_3H,

$$CF_3H\ (+ M) \rightarrow CF_2 + HF\ (+ M) \quad (10)$$

However, our calculations showed that reaction (31) involves a large barrier ($\Delta H_0^o = 224.9$ kJ mol^{-1} at the G3MP2B3 level and $\Delta H_0^o = 252.0$ kJ mol^{-1} at the CBS-QB3 level) which practically rules out reaction (31). The alternative

$$H + CF_3CF_2H \rightarrow H_2 + C_2F_5 \quad (32)$$

is nearly thermoneutral (with[29] $\Delta H_{298}^o = -2.2$ kJ mol^{-1}). We are not aware of kinetic data for this reaction which could be followed by the fast reactions[35]

$$C_2F_5\ (+ M) \rightarrow CF_2 + CF_3\ (+ M) \quad (33)$$

and

$$CF_3 + CF_3CF_2H \rightarrow CF_3H + C_2F_5 \quad (34)$$

thus, supporting a CF_3/C_2F_5 chain and leading to CF_3H. Only fragmentary rate data for reaction (34) have been reported in ref. 36. Therefore, we estimated the rate of reaction (34) by CBS-QB3 calculations and transition state theory to be $k_{34} \approx 1.9 \times 10^{11}$ cm^3 mol^{-1} s^{-1} at 1500 K and $k_{34} \approx 1.3 \times 10^{12}$ cm^3 mol^{-1} s^{-1} at 2000 K. Likewise we estimated $k_{32} \approx 1 \times 10^{13}$ cm^3 mol^{-1} s^{-1} at 1500 K and $k_{32} \approx 2.4 \times 10^{13}$ cm^3 mol^{-1} s^{-1} at 2000 K. Regardless of whether CF_3 is formed through the primary reaction (2) or the sequence (32), (33), under high concentration conditions this mechanism would provide a plausible mechanism for CF_3H formation (at 1500 K and 1000 ppm of C_2F_5H this would lead to a pseudo-first order rate constant for C_2F_5H consumption of about 1.7×10^4 s^{-1}). However, there is an alternative, involving F atoms formed by reaction (28) which could abstract H from C_2F_5H through

$$F + C_2F_5H \rightarrow HF + C_2F_5 \quad (35)$$

With reactions (33) and (34) again a CF_3H-forming chain could be started. Rate constants for reaction (35) can be estimated from ref. 37 and 38, making also this pathway possible under high-concentration conditions (1000 ppm).

It has to be emphasized that the described mechanism is still tentative, although it describes all aspects of our observed CF_2 profiles: overall yield of two CF_2 per decomposed C_2F_5H, slowing down of CF_2 formation at higher concentrations of C_2F_5H by bimolecular reaction of a reaction intermediate (most probably H atoms) with C_2F_5H, and a transition from a higher C_2F_5H decomposition rate, being close to the C_2F_6 decomposition rate at ''low'' concentration, to a rate of the order of the CF_3H decomposition rate at ''high'' concentration. The end products of the decomposition under our conditions then are CF_2, HF, H_2, and H and F atoms, the latter recombining or reacting at longer time scales.

4.2 Decomposition of C_3F_7H

As discussed in Section 3.2 we assume that, under the temperatures and pressures of the present work, the decomposition of C_3F_7H is initiated by the reaction

$$CF_3CFHCF_3\ (+ M) \rightarrow CF_3 + CF_3CFH\ (+ M) \quad (27)$$

Analogous to the C_2F_5H mechanism, CF_3CFH could decompose *via*

$$CF_3CFH\ (+ M) \rightarrow CF_3CF + H\ (+ M) \quad (32)$$

($\Delta H_0^o = 403$ kJ mol^{-1}) and then form 2 CF_2 through the fast sequence of reactions (20) and (3). However, there are more decomposition pathways of CF_3CFH, *e.g.* forming CF_3H + CF ($\Delta H_0^o = 248$ kJ mol^{-1}, rigid activated complex energy 394 kJ mol^{-1}), CF_3 + CFH ($\Delta H_0^o = 372$ kJ mol^{-1}), or CF_2CHF + F ($\Delta H_0^o = 285$ kJ mol^{-1}, all energy values in parentheses from G4MP2 calculations). The energetically most favorable decomposition of CF_3CFH, which does not involve a rigid activated complex, leads to CF_2CHF + F. By decomposition of CF_2CHF also CF_2 would fast be formed and reactions of F and CFH had to be considered. Likewise, reactions of H and CF_3 would have to be taken into account as for C_2F_5H decomposition.

We are not in the position to unravel the described radical mechanism for low reactant concentrations on the basis of CF_2 profiles alone. Likewise, we also cannot uniquely explain which pathways, at higher reactant concentrations, lead to an effective slowing down of CF_2 formation. We note that this is less marked in CF_3CFHCF_3 than in CF_3CF_2H, but it keeps the final CF_2 yield near to three per parent molecule. A comparison with the single-pulse shock study of ref. 2 may be helpful. In this work, much higher reactant concentrations (5000–30 000 ppm) were used and a large variety of final products were identified. Detailed kinetic modeling led to $k_{27} = 10^{15.9} \exp(-355.6\ \text{kJ mol}^{-1}/RT)\ \text{s}^{-1}$ in contrast to $k_{24} = 10^{12.9} \exp(-291.2\ \text{kJ mol}^{-1}/RT)\ \text{s}^{-1}$. Our indications for a radical mechanism, instead of the simple rigid-activated complex mechanism of reaction (24) which after fast decomposition of CF_3CFCF_2 leads to 3 CF_2 + HF, is in agreement with the finding of ref. 2 that k_{27} dominates over k_{24} over the range 1500–1800 K. It also agrees with conclusions from the multiphoton dissociation of $CF_3CF_2CF_2H$ from ref. 17. The lack of an observation of a radical mechanism in ref. 5 and the observation of a dominance of reaction (24), as for C_2F_5H is explained by the low pressures ($<10^{-3}$ Torr) employed.

There remains the question which reactions correspond to the experimental low- and high-concentration values of k_b. Although the low-concentration values of $k_{b,l}$ are close to the value of k_{27} from ref. 2 given above, we are not certain about $k_{b,l} \approx k_{27}$ as CF_2 can be formed by several secondary reactions which probably mostly are slower than reaction (27). Also the high concentration values of k_b, *i.e.* $k_{b,h}$, from our work not necessarily correspond to a retarded release of CF_2 from CF_3H. One may also consider other intermediate ''CF_2 storage''

Table 5 Summary of rate constants (see the text)

Reaction	Rate constant[a]	Note
$C_2F_5H \rightarrow CF_3CF + HF$ (15)	$k_{15,\infty} = 5.5 \times 10^{14} \exp(-42\,800\ K/T)$	[b]
$C_2F_5H \rightarrow CF_2CF_2 + HF$ (16)	$k_{16,\infty} = 2.1 \times 10^{14} \exp(-46\,790\ K/T)$	[b]
$C_2F_5H \rightarrow CF_3H + CF_2$ (18)	$k_{18,\infty} = 1.6 \times 10^{15} \exp(-47\,990\ K/T)$	[b]
$C_2F_5H + Ar \rightarrow CF_3 + CF_2H + Ar$ (19)	$k_{19,\infty} = 5.3 \times 10^{17} \exp(-48\,450\ K/T)$	[c]
	$k_{19,0} = 2.0 \times 10^{18} \exp(-26\,340\ K/T)$	
	$F_{cent,19} = 0.04$	
$CF_3CFHCF_3 \rightarrow CF_3CFCF_2 + HF$ (24)	$k_{24,\infty} = 3.5 \times 10^{15} \exp(-44\,180\ K/T)$	[b]
$CF_3CFHCF_3 \rightarrow CF_3CCF_3 + HF$ (25)	$k_{25,\infty} = 5.9 \times 10^{14} \exp(-48\,610\ K/T)$	[b]
$CF_3CFHCF_3 \rightarrow CF_3H + CF_3CF$ (26)	$k_{26,\infty} = 4.4 \times 10^{14} \exp(-53\,340\ K/T)$	[b]
$CF_3 + Ar \rightarrow CF_2 + F + Ar$ (28)	$k_{28,0} = 3.5 \times 10^{15} \exp(-30\,020\ K/T)$	[d]
$H + CF_3CF_2H \rightarrow H_2 + C_2F_5$ (32)	$k_{32} = 3.3 \times 10^{14} \exp(-5250\ K/T)$	[b]
$CF_3 + CF_3CF_2H \rightarrow CF_3H + C_2F_5$ (34)	$k_{34} = 6.4 \times 10^{14} \exp(-12\,280\ K/T)$	[b]
$CF_2H + Ar \rightarrow CF_2 + HF + Ar$ (10)	$k_{10,\infty} = 1.3 \times 10^{15} \exp(-38\,140\ K/T)$	[e]
	$k_{10,0} = 1.1 \times 10^{16} \exp(-26\,670\ K/T)$	
	$F_{cent,10} = 0.17$	

[a] Rate constants for unimolecular reactions at high pressure in s^{-1}, at low pressure in $cm^3\ mol^{-1}\ s^{-1}$, and for bimolecular reactions in $cm^3\ mol^{-1}\ s^{-1}$. [b] Modeling from this work, see the text and Appendix. [c] Rate constants as for $C_2F_6 + Ar \rightarrow 2\,CF_3 + Ar$, see ref. 33, falloff representation $k_{19}/k_{19,\infty} = [x/(1+x)]F_{cent,19}^{A(x)}$ with $x = k_{19,0}[Ar]/k_{19,\infty}$, $A(x) = 1/[1 + (\log x/N)^2]$ and $N = 2.53$ (at very low pressures, two-channel corrections need to be applied[34]). [d] Low pressure limit, from ref. 21. [e] Rate constants for $CFH_3 + Ar \rightarrow CF_2 + HF + Ar$ from ref. 8. As note c, but with $N = 1.73$.

molecules like C_2F_5H. Our observations of CF_2 alone are not sufficient to draw more detailed conclusions about the identity of the CF_2-storing intermediate species.

5. Conclusions

By monitoring CF_2 production in the thermal decomposition reactions of CF_3CF_2H and CF_3CFHCF_3 under low-concentration, high-pressure, and high-temperature conditions, in our work a closer look at the primary reaction steps was possible than in previous pyrolysis studies. While for C_2F_5H decomposition the rate of the primary C–C bond fission could be identified and found to be close to the rate of C–C bond fission in C_2F_6, similar conclusions could not safely be drawn for C_3F_7H. In both cases the importance of the pressure dependence of the decomposition rates was emphasized. This explains differences between opposing conclusions about the primary reaction steps, derived from high pressure ($>10^3$ Torr) and low pressure experiments ($<10^{-3}$ Torr) in ref. 3, 10, 14 and 5, 11, respectively.

We found that C–C bond fission leading to radical mechanisms always dominated over HF elimination under our conditions. We suspect that this is true down to lower temperatures than assumed in earlier work. We rationalized the unusual slowing down of CF_2 formation with increasing reactant concentrations by bimolecular chain mechanisms which produce intermediate "CF_2-storing" molecules like CF_3H. The latter then release CF_2 at a slower rate than the low-concentration mechanism where such storage molecules are not formed. The conclusions from the present work about the primary decomposition steps and subsequent radical reactions should be implemented into the multi-reaction mechanisms of halon-replacing fire suppressant molecules such as described, *e.g.*, in ref. 3. Conclusions about the primary processes from the low-pressure experiments of ref. 5 and 11 do not appear to be applicable for this purpose.

Although we were not able to obtain precise information on the rate constants of individual elementary reactions, the combination with theoretically modeled rate constants provided an internally consistent picture in agreement with the measurements. In order to facilitate an implementation of our results into large scale modelings of the kinetics, in Table 5 we summarize recommended rate constants from the modelings of the present work. We note substantial differences to previous recommendations. In particular we emphasize that the pressure dependencies of the rates of the primary dissociation reactions cannot be neglected.

Appendix: molecular parameters used in modeling

(Reaction enthalpies are given in Tables 1–4 and in the text).

(a) Harmonic vibrational frequencies

CF_3CF_2H. ν_i/cm^{-1} = 3024, 1424, 1375, 1298, 1220, 1193, 1150, 1141, 861, 715, 575, 570, 514, 407, 355, 235, 201, and free rotor with $\sigma = 3$, and $I_{red} = 36$ amu Å^2; from B3LYP/6-31G(2df,p) calculations scaled by 0.9854 (from G4 model). ν_i/cm^{-1} = 3071, 1422, 1369, 1290, 1191, 1173, 1122, 1121, 852, 710, 570, 567, 511, 407, 354, 239, 206, and free rotor with $\sigma = 3$, and $I_{red} = 36$ amu Å^2; from B3LYP/CBSB7 calculations scaled by 0.99 (from CBS-QB3 model).

CF_3CFHCF_3. ν_i/cm^{-1} = 3037, 1376, 1368, 1298, 1264, 1238, 1218, 1181, 1135, 1121, 901, 677, 599, 544, 527, 509, 447, 337, 318, 285, 232, 220, 162, 91, 22; from B3LYP/6-31G(2df,p) calculations scaled by 0.9854 (from G4MP2 model).

CF_3. ν_i/cm^{-1} = 1229 (2), 1066, 686, 499 (2); from B3LYP/CBSB7 calculations scaled by 0.99 (from CBS-QB3 model).

$CF_3CF_2H \rightarrow CF_3CF + HF$. Transition state ν_i/cm^{-1} = 2052, 1331, 1263, 1247, 1158, 1039, 908, 818, 673, 540, 527, 415, 294, 236, 219, 144, free rotor, and 942i; from B3LYP/6-31G(2df,p) calculations scaled by 0.9854 (from the G4 model).

$CF_3CF_2H \rightarrow CF_2CF_2 + HF$. Transition state ν_i/cm^{-1} = 1725, 1536, 1436, 1263, 1176, 1130, 788, 725, 630, 537, 498, 414, 309,

256, 255, 191, 103, and 1785i; from B3LYP/6-31G(2df,p) calculations scaled by 0.9854 (from the G4 model).

$CF_3CF_2H \rightarrow CF_3H + CF_2$. Transition state ν_i/cm^{-1} = 2735, 1366, 1218, 1209, 1196, 1172, 1039, 735, 630, 581, 507, 502, 263, 209,144, 142, 26, and 1175i; from B3LYP/6-31G(2df,p) calculations scaled by 0.9854 (from the G4 model).

$CF_3CFHCF_3 \rightarrow CF_3CFCF_2 + HF$. Transition state ν_i/cm^{-1} = 1720, 1523, 1428, 1327, 1218, 1200, 1179, 1129, 1013, 787, 763, 700, 608, 589, 536, 495, 412, 367, 340, 277, 261, 236, 197, 161, 76, 51, and 1770i; from B3LYP/6-31G(2df,p) calculations scaled by 0.9854 (from the G4MP2 model).

$CF_3CFHCF_3 \rightarrow CF_3CCF_3 + HF$. Transition state ν_i/cm^{-1} = 3139, 1404, 1328, 1295, 1262, 1223, 1212, 962, 860, 736, 678, 678, 596, 546, 527, 518, 507, 344, 319, 302, 286, 205, 171, 155, 95, 29, and 771i; calculations at the MP2/6-31G(d) level from ref. 12.

$CF_3CFHCF_3 \rightarrow CF_3H + CF_3CF$. Transition state ν_i/cm^{-1} = 2121, 1446, 1349, 1311, 1284, 1262, 1223, 1211, 1036, 870, 807, 699, 665, 564, 521, 519, 515, 430, 282, 254, 245, 195, 185, 128, 81, 52, and 1383i; calculations at the MP2/6-31G(d) level from ref. 12.

$H + CF_3CF_2H \rightarrow H_2 + C_2F_5$. Transition state ν_i/cm^{-1} = 1546, 1355, 1257, 1227, 1203, 1168, 1158, 1095, 808, 692, 591, 572, 510, 413, 357, 296, 294, 219, 205, 58, and 1359i; from B3LYP/CBSB7 calculations scaled by 0.99 (from the CBS-QB3 model).

$CF_3 + CF_3CF_2H \rightarrow CF_3H + C_2F_5$. Transition state ν_i/cm^{-1} = 1458, 1449, 1309, 1206, 1202, 1185, 1179, 1171, 1145, 1075, 874, 740, 690, 594, 573, 521, 504, 503, 414, 356, 253, 205, 197, 185, 136, 73, 40, 32, 5, and 1730i; from B3LYP/CBSB7 calculations scaled by 0.99 (from the CBS-QB3 model).

(b) Rotational constants

CF_3CF_2H. A, B and C/cm^{-1} = 0.123, 0.081 and 0.067; from B3LYP/6-31G(2df,p) calculations (from the G4MP2 model). A, B and C/cm^{-1} = 0.122, 0.080 and 0.066; from B3LYP/CBSB7 calculations (from the CBS-QB3 model).

CF_3CFHCF_3. A, B and C/cm^{-1} = 0.070, 0.035 and 0.031; from B3LYP/6-31G(2df,p) calculations (from the G4MP2 model).

CF_3. A, B and C/cm^{-1} = 0.359, 0.359 and 0.186; from B3LYP/CBSB7 calculations (from the CBS-QB3 model).

$CF_3CF_2H \rightarrow CF_3CF + HF$. Transition state A, B and C/cm^{-1} = 0.109, 0.077 and 0.060; from B3LYP/6-31G(2df,p) calculations (from the G4 model).

$CF_3CF_2H \rightarrow CF_2CF_2 + HF$. Transition state A, B and C/cm^{-1} = 0.106, 0.071 and 0.065; from B3LYP/6-31G(2df,p) calculations (from the G4 model).

$CF_3CF_2H \rightarrow CF_3H + CF_2$. Transition state A, B and C/cm^{-1} = 0.130, 0.060 and 0.051; from B3LYP/6-31G(2df,p) calculations (from the G4 model).

$CF_3CFHCF_3 \rightarrow CF_3CFCF_2 + HF$. Transition state A, B and C/cm^{-1} = 0.064, 0.033 and 0.030; from B3LYP/6-31G(2df,p) calculations (from the G4MP2 model).

$CF_3CFHCF_3 \rightarrow CF_3CCF_3 + HF$. Transition state A, B and C/cm^{-1} = 0.06, 0.04 and 0.03; estimated from the geometry obtained at the MP2/6-31G(d) level from ref. 12.

$CF_3CFHCF \rightarrow CF_3H + CF_3CF$. Transition state A, B and C/cm^{-1} = 0.07, 0.03 and 0.02; estimated from the geometry obtained at the MP2/6-31G(d) level from ref. 12.

$H + CF_3CF_2H \rightarrow H_2 + C_2F_5$. Transition state A, B and C/cm^{-1} = 0.115, 0.076 and 0.065; from B3LYP/CBSB7 calculations (from the CBS-QB3 model).

$CF_3 + CF_3CF_2H \rightarrow CF_3H + C_2F_5$. Transition state A, B and C/cm^{-1} = 0.051, 0.021 and 0.020; from B3LYP/CBSB7 calculations (from the CBS-QB3 model).

Acknowledgements

Helpful discussions with K. Luther are gratefully acknowledged.

References

1 *The SFPE Handbook of Fire Protection Engineering*, ed. P. J. Di Nenno, Nat. Fire Protection Assn., Quincy, MA, USA, 3rd edn, 2002.
2 R. G. Hynes, J. C. Mackie and A. R. Masri, *Combust. Flame*, 1998, **113**, 554.
3 R. G. Hynes, J. C. Mackie and A. R. Masri, *J. Phys. Chem. A*, 1999, **103**, 54.
4 B. A. Williams, D. M. L'Esperance and J. W. Fleming, *Combust. Flame*, 2000, **120**, 160.
5 G. Copeland, E. P. F. Lee, J. M. Dyke, W. K. Chow, D. K. W. Mok and F. T. Chau, *J. Phys. Chem. A*, 2010, **114**, 3540.
6 V. I. Babushok, G. T. Linteris and O. C. Meier, *Combust. Flame*, 2012, **159**, 3569.
7 D. R. Burgess, M. R. Zachariah, W. Tsang and P. R. Westmoreland, *Prog. Energy Combust. Sci.*, 1995, **21**, 453.
8 C. J. Cobos, A. E. Croce, K. Luther and J. Troe, *Z. Phys. Chem.*, 2011, **225**, 1019.
9 V. Aviyente and Y. Inel, *Can. J. Chem.*, 1990, **68**, 1332.
10 K. Takahashi, A. Harada, S. Horigome and T. Inomata, *Combust. Sci. Technol.*, 2007, **179**, 1417.
11 G. Copeland, E. P. F. Lee, J. M. Dyke, W. K. Chow, D. K. W. Mok and F. T. Chau, *J. Phys. Chem. A*, 2010, **114**, 1816.
12 S. D. Peterson and J. S. Francisco, *J. Phys. Chem. A*, 2002, **106**, 3106.
13 G. E. Millward, R. Hartig and E. Tschuikow-Roux, *J. Chem. Soc. D*, 1971, 465.
14 E. Tschuikow-Roux, G. E. Millward and W. J. Quiring, *J. Phys. Chem.*, 3493, **75**, 1971.
15 P. A. Hackett, C. Willis, M. Drouin and E. Weinberg, *J. Phys. Chem.*, 1873, **84**, 1980.
16 S. Kato, Y. Makide, K. Takeuchi and T. Tominaga, *J. Phys. Chem.*, 3977, **88**, 1984.
17 S. Kato, Y. Makide, T. Tominaga and K. Takeuchi, *J. Phys. Chem.*, 4278, **91**, 1987.

18 C. J. Cobos, A. E. Croce, K. Luther, L. Sölter, E. Tellbach and J. Troe, *J. Phys. Chem. A*, 2013, **117**, 11420.
19 T. Yamamoto, A. Yasuhara, F. Shiraishi, K. Kaya and T. Abe, *Chemosphere*, 1997, **35**, 643.
20 Ch. Kappel, K. Luther and J. Troe, *Phys. Chem. Chem. Phys.*, 2002, **4**, 4392.
21 C. J. Cobos, A. E. Croce, K. Luther and J. Troe, *J. Phys. Chem. A*, 2010, **114**, 4755.
22 A. D. Boese and J. M. L. Martin, *J. Chem. Phys.*, 2004, **121**, 3405.
23 Y. Zhao and D. G. Truhlar, *Theor. Chem. Acc.*, 2008, **120**, 215.
24 J. A. Montgomery, M. J. Frisch, J. W. Ochterski and G. A. Petersson, *J. Chem. Phys.*, 1999, **110**, 2822.
25 A. G. Baboul, L. A. Curtiss, P. C. Redfern and K. Raghavachari, *J. Chem. Phys.*, 1999, **110**, 7650.
26 L. A. Curtiss, P. C. Redfern and K. Raghavachari, *J. Chem. Phys.*, 2007, **127**, 124105.
27 L. A. Curtiss, P. C. Redfern and K. Raghavachari, *J. Chem. Phys.*, 2007, **126**, 084108.
28 M. J. Frisch, *et al.*, *Gaussian 09, Revision A.02-SMP*, Gaussian Inc., Wallington, CT, 2009.
29 E. Goos, A. Burcat and B. Ruscic, Extended Third Millenium Ideal Gas and Condensed Phase Thermochemical Data Base for Combustion with Updates from Active Thermochemical Tables, ftp.technion.ac.il/pub/supported/aetdd/, update July 17, 2013.
30 J. Troe, *J. Phys. Chem.*, 1979, **83**, 114.
31 J. Troe and Ber. Bunsenges, *Phys. Chem.*, 1983, **87**, 161.
32 R. G. Gilbert, K. Luther, J. Troe and Ber. Bunsenges, *Phys. Chem.*, 1983, **87**, 169.
33 C. J. Cobos, A. E. Croce, K. Luther and J. Troe, *J. Phys. Chem. A*, 2010, **114**, 4748.
34 Th. Just and J. Troe, *J. Phys. Chem.*, 1980, **84**, 3068.
35 K. Li, E. M. Kennedy and B. Z. Dlugorski, *Chem. Eng. Sci.*, 2000, **55**, 4067.
36 R. D. Giles, L. M. Quick and E. Whittle, *Trans. Faraday Soc.*, 1967, **63**, 662.
37 T. J. Wallington, M. D. Hurley, J. Shi, M. M. Maricq, J. Sehested, O. J. Nielsen and T. Ellermann, *Int. J. Chem. Kinet.*, 1993, **25**, 651.
38 X. L. Zhao, Y. M. Ji, Z. S. Li, Y. Wang and J. Y. Liu, *THEOCHEM*, 2007, **808**, 17.